NANO LETTERS

Letter

pubs.acs.org/NanoLett

# Highly Cyclable Lithium–Sulfur Batteries with a Dual-Type Sulfur Cathode and a Lithiated Si/SiO$_x$ Nanosphere Anode

Sang-Kyu Lee,[†] Seung-Min Oh,[†] Eunjun Park,[†] Bruno Scrosati,[§] Jusef Hassoun,[¶] Min-Sik Park,[‡] Young-Jun Kim,[‡] Hansu Kim,*[,†] Ilias Belharouak,[∥] and Yang-Kook Sun*[,†]

[†]Department of Energy Engineering, Hanyang University, 222 Wangsimni-ro, Seongdong-gu, Seoul 133-791, South Korea

[‡]Advanced Batteries Research Center, Korea Electronic Technology Institute, 68 Yatap-dong, Bundang-gu, Seongnam 463-816, South Korea

[§]Italian Institute of Technology, Via Morego, 30 16163 Genova, Italy

[¶]Department of Chemistry, University of Rome Sapienza, Piazzale Aldo Moro, 5, 00185, Rome, Italy

[∥]Qatar Environment and Energy Research Institute, Qatar Foundation, P.O. Box 5825, Doha, Qatar

Supporting Information

**ABSTRACT:** Lithium–sulfur batteries could become an excellent alternative to replace the currently used lithium-ion batteries due to their higher energy density and lower production cost; however, commercialization of lithium–sulfur batteries has so far been limited due to the cyclability problems associated with both the sulfur cathode and the lithium–metal anode. Herein, we demonstrate a highly reliable lithium–sulfur battery showing cycle performance comparable to that of lithium-ion batteries; our design uses a highly reversible dual-type sulfur cathode (solid sulfur electrode and polysulfide catholyte) and a lithiated Si/SiO$_x$ nanosphere anode. Our lithium–sulfur cell shows superior battery performance in terms of high specific capacity, excellent charge–discharge efficiency, and remarkable cycle life, delivering a specific capacity of ~750 mAh g$^{-1}$ over 500 cycles (85% of the initial capacity). These promising behaviors may arise from a synergistic effect of the enhanced electrochemical performance of the newly designed anode and the optimized layout of the cathode.

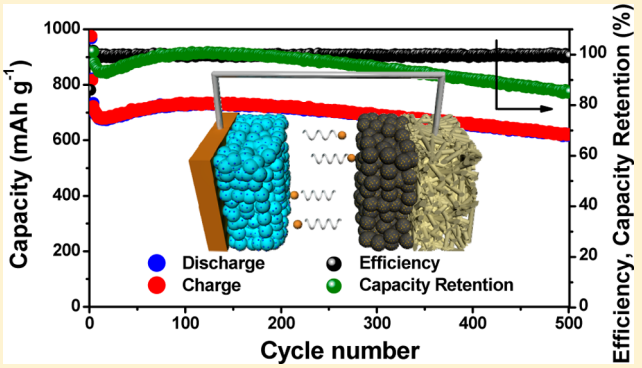


**KEYWORDS:** *Lithium–sulfur battery, polysulfide-catholyte, silicon-based anode, full cell, hybrid cathode*

The lithium–sulfur battery is one of the most promising high-energy-density electrochemical energy storage system for emerging applications such as power storage systems for renewable energy plants and the powering of sustainable electric vehicles.[1,2] The natural abundance and low cost of sulfur, coupled with the high theoretical energy density of sulfur-based cathodes, viz., 1675 mAh g$^{-1}$ and 2500 Wh kg$^{-1}$, are the major advantages of sulfur-based batteries.[3−9] However, the insulating nature of sulfur leads to low active material utilization, and sulfur electrodes have low stability due to the formation of soluble lithium polysulfides during cell operation; these problems have so far limited the commercialization of lithium–sulfur batteries.[10−12] There has been consistent progress recently toward optimizing the sulfur electrodes, for example, by the use of conductive carbonaceous matrices[13] and metal–organic framework (MOF) for sulfur impregnation,[14−18] as well as by the choice of suitable electrolytes.[19−21] Recently, several research groups have reported that the addition of lithium polysulfide to the electrolyte could improve the performance of the Li/S batteries in terms of cycle performance and energy density.[19−27]

Another major concern regarding the lithium–sulfur battery system is its use of a lithium–metal anode, which is well-known to have some critical problems including chemical reactivity in commonly used organic electrolytes and dendritic growth of lithium during cycling, leading to poor cycle performance and safety problems. In addition, when coupled with a sulfur cathode, the lithium metal anode reacts with lithium polysulfide to form an insoluble $Li_2S$ phase on lithium–metal surface, leading to the loss of lithium metal and eventually causing poor cycle performance of the system. To minimize the problems associated with lithium–metal anode an excess amount of lithium metal usually is needed to construct the full cell to secure its long cycle life, which might lead to degradation of both the energy density and the safety of the full cell. Recently, alloy-type anode materials have been suggested as alternatives to replace the lithium–metal anode. However, even though some examples have shown promise for practical use with sulfur

**Received:** November 20, 2014
**Revised:** March 26, 2015





DOI: 10.1021/nl504460s
*Nano Lett.* XXXX, XXX, XXX−XXX

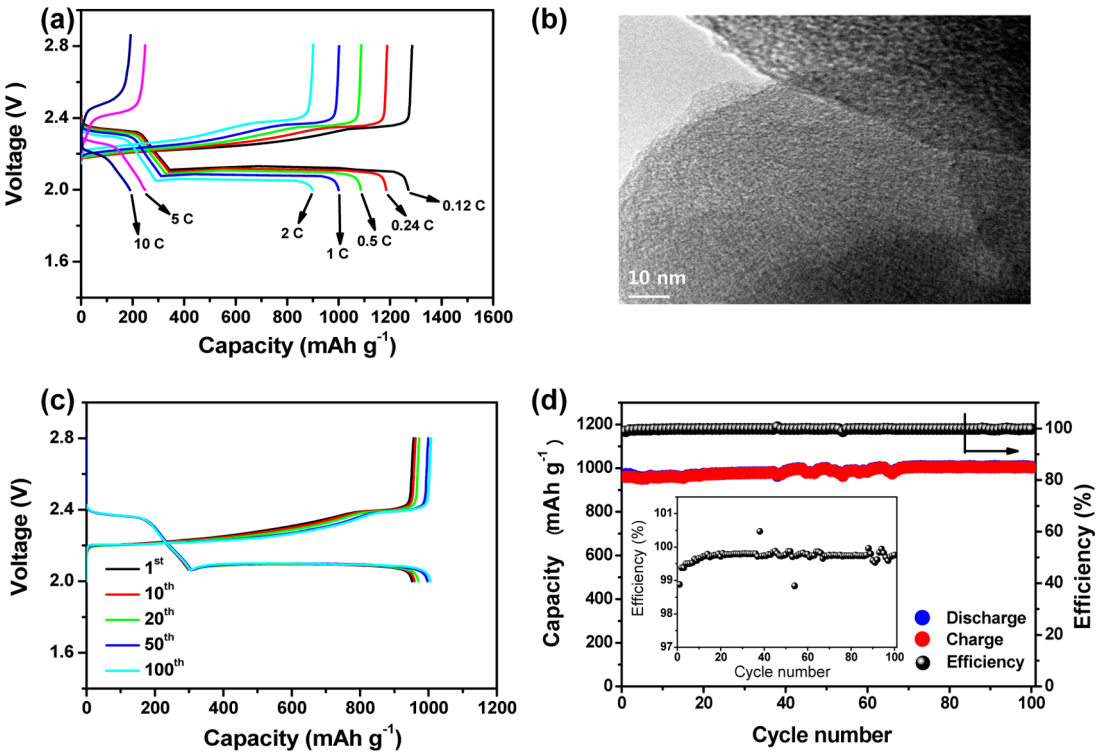


**Figure 1.** (a) Voltage profiles of the dual-type sulfur cathode with a catholyte; the C-rate was varied from 0.12C to 10C, where 1C = 1675 mAh $g^{-1}$ versus the overall sulfur weight, and the voltage ranged from 2.8 to 2.0 V. (b) TEM image of sulfur-activated carbon composite particles. (c) Voltage profiles and (d) cycling responses of the same cell cycled at a rate of C/3. Inset: magnification of Coulombic efficiency.

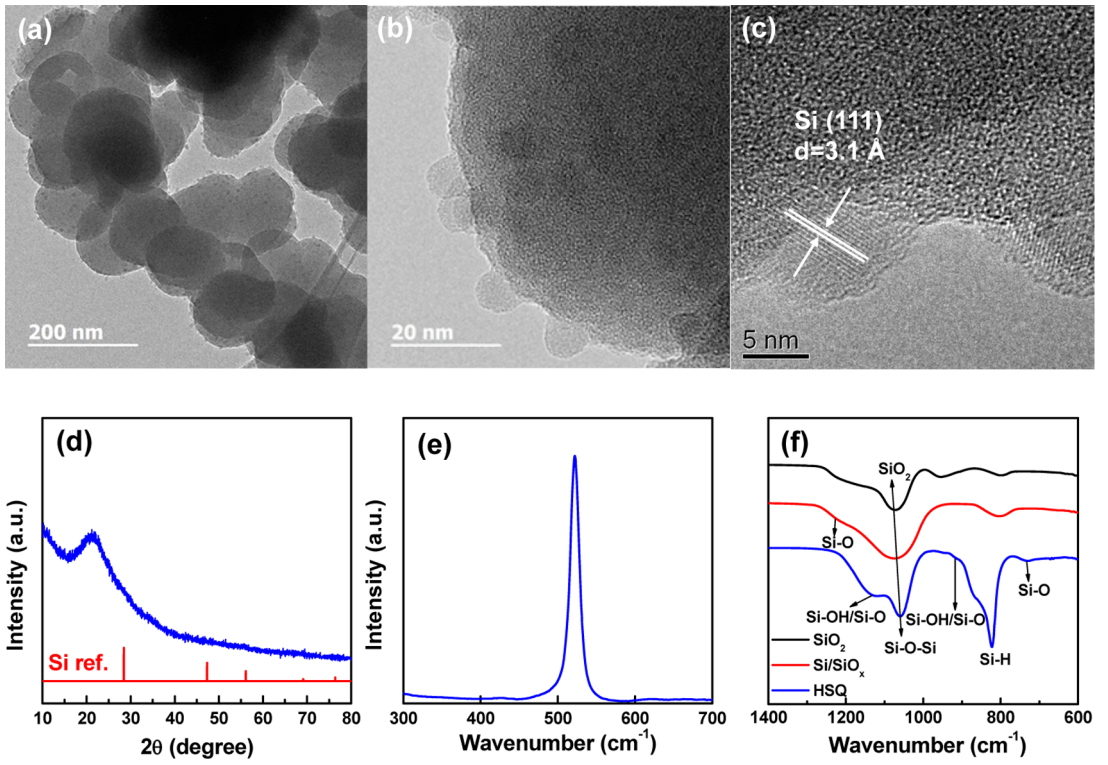


**Figure 2.** (a,b) TEM images of Si/$SiO_x$ nanosphere. (c) HR TEM image of Si/$SiO_x$ nanosphere, (d) XRD patterns, (e) Raman spectrum, and (f) FTIR spectrum of Si/$SiO_x$ nanosphere materials.

cathodes, the cycle performance and the energy density of lithium−sulfur battery system adopting alloy-type anode materials needs to be advanced further before they can penetrate the rechargeable battery market.



DOI: 10.1021/nl504460s
*Nano Lett.* XXXX, XXX, XXX−XXX

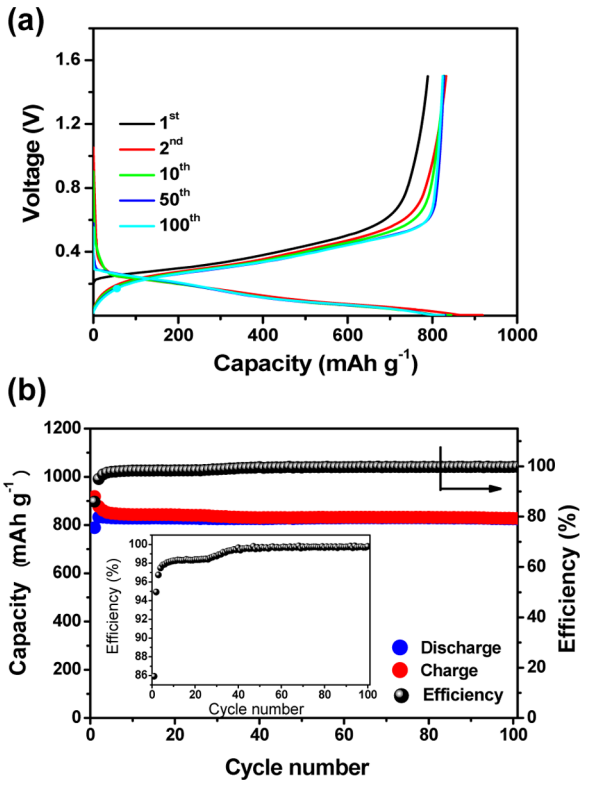


**Figure 3.** (a) Voltage profiles and (b) cycling performance of lithiated $Si/SiO_x$ nanosphere anode with a catholyte. Current, 200 mA $g^{-1}$; voltage range, 1.5–0.005 V; temperature, 30 °C. Inset: magnification of Coulombic efficiency.

Herein we demonstrate a lithium–sulfur cell configuration with a newly designed dual-type hybrid sulfur cathode and a lithiated $Si/SiO_x$ nanosphere anode with an optimized liquid electrolyte. Our hybrid dual-type sulfur cathode consists of an activated carbon–sulfur composite on a gas diffusion layer (GDL) electrode in contact with a catholyte solution to which $Li_2S_8$ has been added. This cathode system delivers a maximum capacity of ~1300 mAh $g^{-1}$ with respect to the overall mass of sulfur (about 1.2 mg) from both the solid sulfur (about 0.2 mg on the electrode) and the dissolved lithium polysulfide (1.024 mg in 80 $\mu$L of the polysulfide-containing electrolyte). At a rate of C/3, our dual-type cathode shows a capacity of ~1000 mAh $g^{-1}$, Coulombic efficiencies of more than 99.3% except for the first cycle and a maintenance of the capacity above 99% of the initial capacity even after 100 cycles. The lithiated $Si/SiO_x$ nanosphere anode used shows highly stable cycling behavior over 100 cycles with a capacity of as high as 800 mAh $g^{-1}$ and cycling efficiency approaching 100%. The full lithium-ion sulfur cell presented herein delivers a capacity of ~750 mAh $g^{-1}$ with an average working voltage of about 1.8 V, corresponding to the energy density of 497 Wh $kg^{-1}$ based on the weight of active materials on the cathode and anode. This energy density would be more than double that of the commercially available lithium-ion batteries. Besides its high energy density, the lithium–sulfur full cell demonstrated here shows cycle performance comparable to that of commercial lithium-ion batteries. We believe that these results might advance the development of practical lithium–sulfur batteries, particularly for use in emerging markets, including portable devices, electric vehicles, and large-scale power storage systems for renewable energies.

Figure 1a shows the voltage profiles of the dual-type sulfur electrodes presented here at a series of C-rates; these electrodes consisted of sulfur infiltrated activated carbon particles (Figure 1b; Supporting Information Figure S1, S2) coated onto the surface of a gas-diffusion-layer (GDL) current collector and were coupled with $Li_2S_8$-containing electrolyte as a liquid cathode. At the rate of C/3, the dual-type sulfur electrode shows a reversible capacity of ~1000 mAh $g^{-1}$, arising not only from the redox reaction of solid sulfur, but also from that of the polysulfide dissolved in the electrolyte, which occurs on the surfaces of both the GDL and the activated carbon particles. When a composite of solid sulfur and activated carbon was used on a conventional Al foil current collector instead of a GDL, the reversible capacity decreased to as low as 607 mAh $g^{-1}$ (Supporting Information Figure S3), implying that the GDL acts as a reaction site for the redox reaction of the polysulfide as well as a current collector. Figure 1d shows the excellent capacity retention of the dual-type sulfur cathode over 100 cycles with Coulombic efficiencies of more than 99.3% except for the first cycle. Slight increase of the capacity during cycling can be attributed to the redistribution of polysulfides in the cathode because of very high surface area of the activated carbon (Supporting Information Figure S2).[27] Note that the voltage profiles of the dual-type sulfur cathode at various C-rates show relatively low polarization loss; increasing the C-rate from 0.12C to 2C decreases the capacity from 1200 to 900 mAh $g^{-1}$ (Figure 1a).

A full lithium–sulfur cell was constructed by employing a lithiated $Si\text{-}SiO_x$ nanosphere anode characterized by high performance in terms of both capacity and cycle life. Figure 2 shows the properties of the $Si\text{-}SiO_x$ nanosphere materials prepared by a pyrolysis of hydrogen silsesquioxane ($HSiO_{1.5}$, HSQ) nanosphere that was obtained by a sol–gel reaction of triethoxysilane. Figure 2a,b shows that the resulting material has a well-defined spherical morphology with a size of about 200 nm and mainly consists of amorphous nonstoichiometric silicon oxide ($SiO_x$), which is supported by the XRD pattern in Figure 2d. However, the high-resolution transmission electron microscopy (TEM) image of the $Si\text{-}SiO_x$ material (Figure 2c) shows crystals of about 5 nm in size on the surface of the nanosphere. The *d* spacing of the observed crystals on the surface of amorphous nanosphere was about 3.1 Å, which corresponds to crystalline Si(111). Raman spectroscopy shows a strong peak at 520 $cm^{-1}$, which is the characteristic peak of long-range-ordered crystalline silicon (Figure 2e). Figure 2f compares the FTIR spectra of the HSQ nanosphere, $Si/SiO_x$ nanosphere obtained from heat treatment of HSQ, and $SiO_2$ as a reference. After heat treatment, the band corresponding to Si–H bond observed at 825 $cm^{-1}$ disappeared, which might be due to the thermal decomposition of HSQ into an amorphous $SiO_x$ phase and Si nanocrystals with a size of about 5 nm.[28] Lithiated $Si\text{-}SiO_x$ nanosphere here reported is expected to deliver high capacity that is stable over prolonged cycling because the amorphous $SiO_x$ matrix phase (~200 nm) together with the nanoscale Si (~5 nm) could accommodate the huge volume changes of silicon occurring during the lithium-alloying and dealloying processes. Prior to cycling, the $Si\text{-}SiO_x$ nanosphere was fully lithiated by direct contact with lithium metal foil in the electrolyte, as reported previously,[29] allowing its use as the lithium source in a lithiated $Si\text{-}SiO_x/S$ full cell. The voltage profile of the lithiated silicon electrode in the lithium half cell shows very stable behavior with an average working voltage of about 0.3 V versus Li, reflecting the Li–Si


DOI: 10.1021/nl504460s
Nano Lett. XXXX, XXX, XXX–XXX

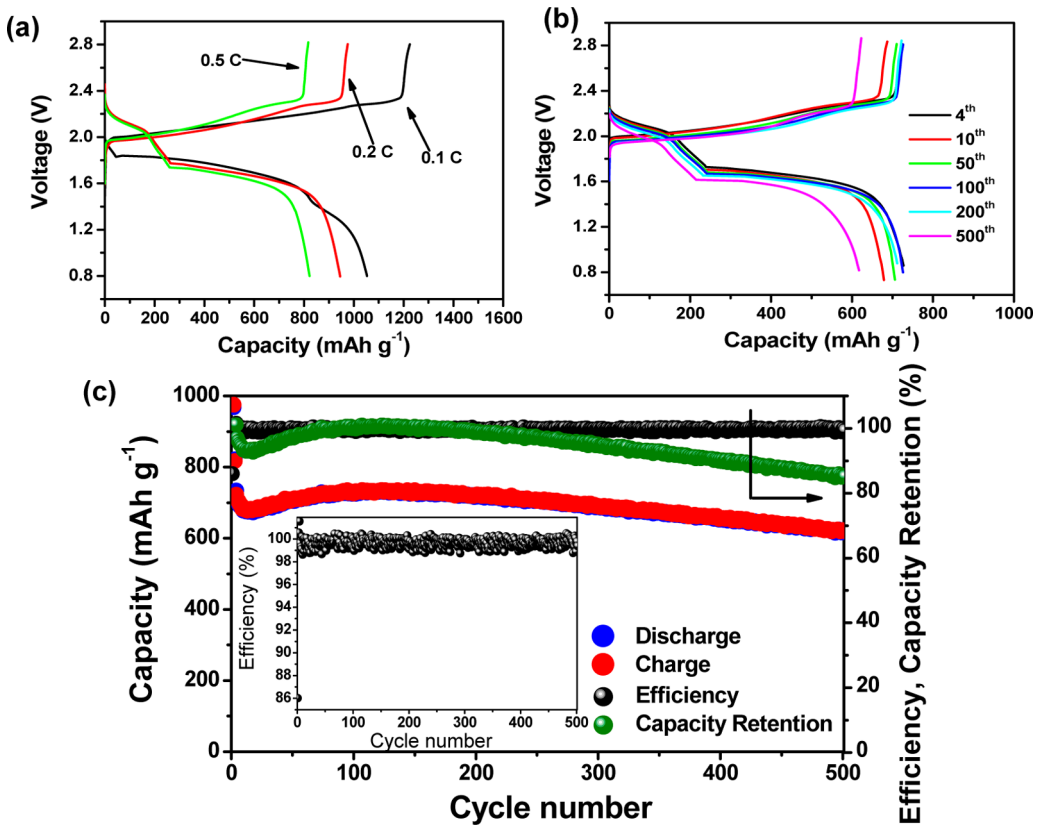


**Figure 4.** (a) Voltage profiles of the full cell adopting the lithiated Si-$SiO_x$ nanosphere/DME/DOL (1:1 v/v), $Li_2S_8$ (0.05 M), LiTFSI (1 M), $LiNO_3$ (0.4 M)/AC-S structure and including a GDL current collector, cycled at 0.1C (black curve), 0.2C (red curve), and 0.5C (green curve) rates. (b) Voltage profiles and (c) cyclic responses of the lithiated Si-$SiO_x$/DME/DOL (1:1 v/v), $Li_2S_8$ (0.05 M), LiTFSI (1 M), $LiNO_3$ (0.4 M)/AC-S full cell cycled at 1C rate. The upper and lower voltage limits are, respectively, 2.8 and 0.8 V. 1C = 1675 mAh $g^{-1}$ versus overall sulfur weight; temperature, 30 °C. Inset: magnification of Coulombic efficiency.

alloying process and a specific capacity of as high as 830 mAh $g^{-1}$ at the current of 200 mA $g^{-1}$ (Figure 3a,b). The cycling behavior of the cell shows highly stable capacity retention over 100 cycles with Coulombic efficiencies of more than 98% except for the initial few cycles. These excellent electrochemical performances of the lithiated Si-$SiO_x$ nanosphere electrode, enabled by nanoarchitecturing using a nanoscale Si crystal and an amorphous $SiO_x$ nanosphere as building blocks, suggest that our anode material presented herein would provide sufficient electrochemical performance as a high-capacity anode to replace the metallic lithium anode in a full lithium−sulfur battery.

Figure 4 shows the electrochemical performance of the full cell with the dual-type sulfur cathode and the lithiated Si-$SiO_x$ nanosphere anode. Figure 4a shows the voltage profiles of the full cell cycled at a rate of 0.1C (black curve), 0.2C (red curve), and 0.5C (green curve). The cell delivers a specific capacity of 1100 mAh $g^{-1}$ at a 0.1C-rate with an average voltage of about 1.8 V. Further increase in the C-rate up to 1C produces only a minor decrease in the specific capacity to 750 mAh $g^{-1}$ (Figure 4b). On the basis of the cell capacity obtained at a rate of 1C with the weight of the electrode materials, the estimated energy density of this full cell is 497 Wh $kg^{-1}$. The resulting energy density of our full cell is more than double that of the commercially available lithium-ion batteries. It should be noted that the full cell maintained about 85.5% of its specific capacity over 500 cycles with cycling efficiencies of more than 98.2% except for the first cycle (86%) (Figure 4c), implying that the cycle life of the full cell reported herein nearly reaches almost that of commercial lithium-ion battery. The excellent cycle performance of the cell arises from both the newly designed anode as well as the dual-type sulfur cathode, that is, hybrid of solid sulfur and polysulfide catholyte, used in this work.

We observed the morphological changes of Si/$SiO_x$ as well as the thickness changes of the Si/$SiO_x$ electrode before and after the prelithiation of Si/$SiO_x$ using a scanning electron microscopy (SEM) (Figure 5). As shown in Figure 5a−c, SEM observation shows that the diameter of Si/$SiO_x$ nanosphere increased from 200 nm (before prelithiation) to 300 nm (after prelithiation) (Figure 5a,b) and compared to the pristine lithiated Si/$SiO_x$ nanosphere materials, the cycled anode material retained its initial morphology without any mechanical damage including cracking and pulverization (Figure 5b,c). Cross-sectional images of the Si/$SiO_x$ electrode show that the thickness of the Si/$SiO_x$ electrode increased about 4 $\mu$m after prelithiation (Figure 5d,e), which was probably due to the expansion of Si/$SiO_x$ nanosphere as shown in Figure 5e. The dimensional stability of a lithiated Si/$SiO_x$ electrode was also investigated through the observation of the thickness changes of the electrode after cycling. Figure 5e,f shows cross-sectional SEM images of lithiated Si/$SiO_x$ electrode before and after 20 cycles. Even after 20 cycles, the lithiated Si/$SiO_x$ electrode maintained almost its original thickness without any crack. These results clearly show that the nanoscale engineering of Si and the use of amorphous $SiO_x$ as a matrix here effectively mitigates the mechanical strains


DOI: 10.1021/nl504460s
Nano Lett. XXXX, XXX, XXX−XXX

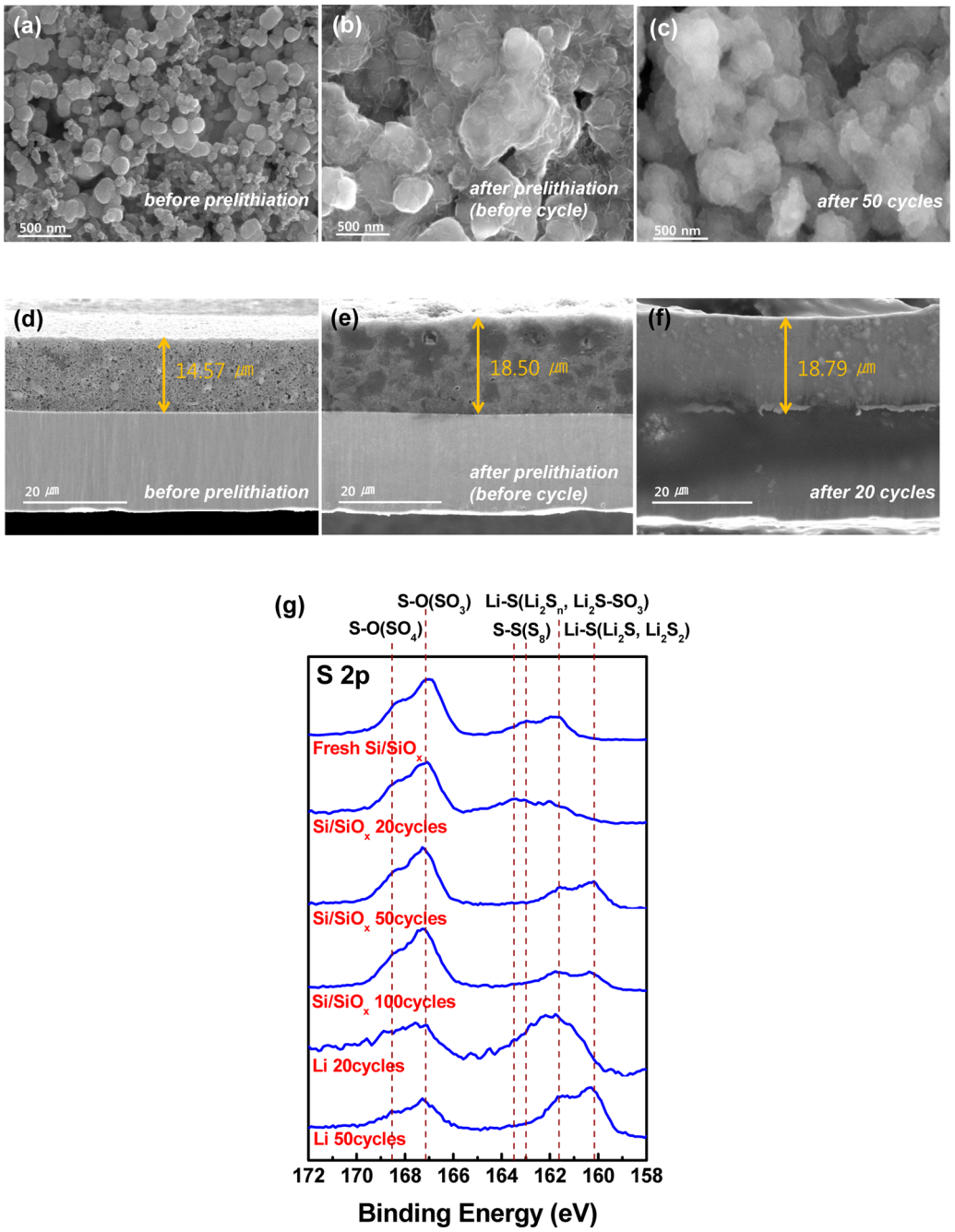


**Figure 5.** SEM images of (a) before prelithiation electrode, (b) fresh lithiated Si/$SiO_x$ nanosphere electrode, and (c) the Si/$SiO_x$ nanosphere electrode cycle performance after 50 cycles. FESEM images of Si/$SiO_x$ electrode: cross sectional view (d) before prelithiation, (e) before cycling, and (f) after 20 cycles. (g) XPS spectra of the Si/$SiO_x$ electrode before and after cycling and lithium−metal electrode after cycling.

induced by the huge volume changes of Si during cycling. Given that the activity of lithium in the Li−Si alloy phase is less than that of metallic lithium, one can reasonably expect that unwanted side reaction between polysulfide and lithium can be suppressed in the lithiated Si/$SiO_x$ anode.[29] Figure 5g shows the X-ray photoelectron spectroscopy (XPS) spectra of the cycled lithiated Si/$SiO_x$ electrode and metallic lithium electrode. Because $LiNO_3$ as an additive plays a role in minimizing the side reactions of polysulfide with lithium, the peaks corresponding to $Li_2S$ were not observed at either metallic lithium electrode or lithiated Si/$SiO_x$ electrode up to 20 cycles. After 50 cycles, however, the XPS spectrum of the lithium−metal electrode shows obvious strong XPS peaks corresponding to $Li_2S$ phase,[26,30−32] indicating that the repeated deposition and stripping of lithium during cycling results in mechanical damage of the solid electrolyte interface (SEI) film of lithium metal electrode, thus leading to the exposure of lithium metal to the polysulfide dissolved in the electrolyte and the formation of insoluble $Li_2S$ phase. By contrast, although the peaks corresponding to $Li_2S$ phase were also observed, the XPS spectrum of lithiated Si/$SiO_x$ electrode after 50 cycles shows relatively much weaker peaks corresponding $Li_2S$ phase compared to those of lithium−metal electrode. These results can be attributed to the reduced chemical activity of lithiated Si/$SiO_x$ material compared to metallic lithium as well as the aforementioned dimensional stability of the lithiated


DOI: 10.1021/nl504460s
Nano Lett. XXXX, XXX, XXX−XXX

$Si/SiO_x$ electrode. The latter might enable highly stable SEI film formation on the anode and the former would mitigate the loss of active material (polysulfide in the electrolyte) during cycling.

In summary, we have reported a lithium−sulfur full cell using a dual-type (solid sulfur-polysulfide catholyte) sulfur cathode and a lithiated $Si-SiO_x$ nanosphere anode, showing cycling performance comparable to that of the commercially available lithium-ion batteries and energy density higher than that of lithium-ion batteries. Both the cathodic and anodic half cells used herein demonstrated excellent performances in terms of reversible capacity, cycle life, and cycling efficiency over repeated cycles. The full cell adopting this couple showed a capacity of 750 mAh $g^{-1}$ at a C-rate of as high as 1C (1675 mA $g^{-1}$) with an average working voltage of 1.8 V and maintained more than 85% of its initial capacity after 500 cycles. We firmly believe that this cell configuration, when coupled with the newly designed electrode materials, represents a significant step toward the realization of commercially available lithium−sulfur battery technology.

## ■ ASSOCIATED CONTENT

### Supporting Information

Additional information and figures. This material is available free of charge via the Internet at http://pubs.acs.org.

## ■ AUTHOR INFORMATION


### Corresponding Authors

*E-mail: khansu@hanyang.ac.kr.
*E-mail: yksun@hanyang.ac.kr.


### Notes

The authors declare no competing financial interest.

## ■ ACKNOWLEDGMENTS

This work was supported in part by a grant from the Human Resources Development Program (No. 20124010203310) of the Korea Institute of Energy Technology Evaluation and Planning, funded by the Korean government, by the Ministry of Trade, Industry and Energy, by a National Research Foundation of Korea grant funded by the Korean government (MEST) (No. 2009-0092780), and in part by the research fund of Hanyang University (HY-2012-T).

## ■ REFERENCES


(1) Scrosati, B.; Hassoun, J.; Sun, Y.-K. *Energy Environ. Sci.* **2011**, *4*, 3287−3295.
(2) Peled, E.; Sternberg, Y.; Gorenshtein, A.; Lavi, Y. *J. Electrochem. Soc.* **1989**, *136*, 1621−1625.
(3) Peled, E.; Gorenshtein, A.; Segal, M.; Sternberg, Y. *J. Power Sources* **1989**, *26*, 269−271.
(4) Bruce, P. G. *Solid State Ionics* **2008**, *179*, 752−760.
(5) Ji, X.; Lee, K.-T.; Nazar, L. F. *Nat. Mater.* **2009**, *8*, 500−506.
(6) Hassoun, J.; Scrosati, B. *Angew. Chem., Int. Ed.* **2010**, *49*, 2371−2374.
(7) Ji, X.; Nazar, L. F. *J. Mater. Chem.* **2010**, *20*, 9821−9826.
(8) Rao, M.; Li, W.; Cairns, E. J. *Electrochem. Commun.* **2012**, *17*, 1−7.
(9) Jayaprakash, N.; Shen, J.; Moganty, S. S.; Corona, A.; Archer, L. A. *Angew. Chem., Int. Ed.* **2011**, *50*, 5904−5908.
(10) Mikhaylik, Y. V.; Akridge, J. R. *J. Electrochem. Soc.* **2004**, *151*, A1969−A1976.
(11) Ryu, H. S.; Guo, Z.; Ahn, H. J.; Cho, G. B.; Liu, H. *J. Power Sources* **2009**, *189*, 1179−1183.
(12) Barchasz, C.; Molton, F.; Duboc, C.; Leprêtre, J. C.; Patoux, S.; Alloin, F. *Anal. Chem.* **2012**, *84*, 3973−3980.
(13) Hassoun, J.; Agostini, M.; Latini, A.; Panero, S.; Sun, Y.-K.; Scrosati, B. *J. Electrochem. Soc.* **2012**, *159*, A390−A395.
(14) Zhang, C.; Wu, H. B.; Yuan, C.; Guo, Z.; Lou, X. W. *Angew. Chem., Int. Ed.* **2012**, *51*, 9592−9595.
(15) He, G.; Ji, X.; Nazar, L. F. *Energy Environ. Sci.* **2011**, *4*, 2878−2883.
(16) Wang, H.; Yang, Y.; Liang, Y.; Robinson, J. T.; Li, Y.; Jackson, A.; Cui, Y.; Dai, H. *Nano Lett.* **2011**, *11*, 2644−2647.
(17) Kim, J.; Lee, D.-J.; Jung, H.-G.; Sun, Y.-K.; Hassoun, J.; Scrosati, B. *Adv. Funct. Mater.* **2013**, *23*, 1076−1080.
(18) Demir-Cakan, R.; Morcrette, M.; Nouar, F.; Davoisne, C.; Devic, T.; Gonbeau, D.; Dominko, R.; Serre, C.; Férey, G.; Tarascon, J.-M. *J. Am. Chem. Soc.* **2011**, *133*, 16154−16160.
(19) Aurbach, D.; Pollak, E.; Elazari, R.; Salitra, G.; Kelley, C. S.; Affinito, J. *J. Electrochem. Soc.* **2009**, *156*, A694−A702.
(20) Xiong, S.; Xie, K.; Diao, Y.; Hong, X. *Electrochim. Acta* **2012**, *83*, 78−86.
(21) Chen, S.; Dai, G.; Gordin, M. L.; Wang, D. *RSC Adv.* **2013**, *3*, 3540−3543.
(22) Demir-Cakan, R.; Morcrette, M.; Gangulibabu; Guéguen, A.; Dedryvère, R.; Tarascon, J.-M. *Energy Environ. Sci.* **2013**, *6*, 176−182.
(23) Suo, L.; Hu, Y.-S.; Li, H.; Armand, M.; Chen, L. *Nat. Commun.* **2013**, *4*, 1481.
(24) Yang, Y.; Zheng, G.; Cui, Y. *Energy Environ. Sci.* **2013**, *6*, 1552−1558.
(25) Aurbach, D. *J. Power Sources* **2000**, *89*, 206−218.
(26) Bruce, P. G.; Evans, J.; Vincent, C. A. *Solid State Ionics* **1988**, *28−30*, 918−922.
(27) Yao, H.; Zheng, G.; Hsu, P.-C.; Kong, D.; Cha, J. J.; Li, W.; Seh, Z. W.; McDowell, M. T.; Yan, K.; Liang, Z.; Narasimhan, V. K.; Cui, Y. *Nat. Commun.* **2014**, *5*, 3943.
(28) Belot, V.; Corriu, R.; Leclercq, D.; Mutin, P. H.; Vioux, A. *Chem. Mater.* **1991**, *3*, 127−131.
(29) Hassoun, J.; Kim, J.; Lee, D.-J.; Jung, H.-G.; Lee, S.-M.; Sun, Y.-K.; Scrosati, B. *J. Power Sources* **2012**, *202*, 308−313.
(30) Wagner, C. D.; Naumkin, A. V.; Kraut-Vass, A.; Allison, J. W.; Powell, C. J.; Rumble, J. R. Nist X-ray Photoelectron Spectroscopy Database. *NIST Standard Reference Database 20, Version 3.5*; National Institute of Standards and Technology: Gaithersburg, MD, http://srdata.nist.gov/xps/ 2007.
(31) Diao, Y.; Xie, K.; Xiong, S.; Hong, X. *J. Power Sources* **2013**, *235*, 181−186.
(32) Xiong, S.; Xie, K.; Diao, Y.; Hong, X. *J. Power Sources* **2014**, *246*, 840−845.




DOI: 10.1021/nl504460s
*Nano Lett.* XXXX, XXX, XXX−XXX